Int J Adv Manuf Technol (2017) 91:1297–1307
DOI 10.1007/s00170-016-9818-3

ORIGINAL ARTICLE

Influence of finish milling parameters on machined surface integrity and fatigue behavior of Ti1023 workpiece

Xun Li[1] · **Peng Zhao**[1] · **Yongsong Niu**[1] · **Chunming Guan**[1]

Received: 6 July 2016 / Accepted: 21 November 2016 / Published online: 5 December 2016

Abstract Ti1023 is a high specific strength material, widely used for manufacturing load-bearing workpieces in aerospace, aviation, and other fields, of which the main failure mode is fatigue fracture. Milling is the main process of Ti1023 complex structure parts, and the surface integrity generated has a significant impact on the fatigue life. Based on the deep mechanism analysis on the surface topography and surface roughness formation, the influence of the finish milling parameters on the machined surface integrity and the fatigue life of specimens is obtained. By conducting the milling experiments, the influence of surface roughness, surface microhardness, and surface residual stress on the fatigue life of specimens is analyzed. Results show that milling speed v_s is the predominating parameter affecting the fatigue performance of Ti1023 irrespective of the tool wear; the essential reason of which is the surface enhancement caused by surface microhardening rate and the thickness of microstructural deforming layer underneath the machined surface. Although the feed per tooth f_z obviously influences the surface roughness, it has little effect on the surface stress concentration factor. Therefore, f_z is not decisive to the fatigue performance of the specimen. The research results provide guidelines on the optimization of finish milling parameters of Ti1023, as well as a theoretical basis for the anti-fatigue investigation of Ti1023 parts.

✉ Xun Li
lixun@buaa.edu.cn; lixunbuaa@163.com

[1] School of Mechanical Engineering and Automation, Beihang University, Beijing 100191, China

Keywords Surface integrity · Fatigue · Milling · Surface roughness · Titanium alloy

1 Introduction

Ti1023 is a kind of β-type titanium alloy which has high strength, low forging temperature, and strong resistance to corrosion. When utilizing Ti1023 instead of equal strength 20CrMnSiA and TC4 in aircraft fuselage, wings, and landing gear structures, the weight could be reduced by 40 and 20%, respectively [1]. Therefore, Ti1023 is widely used in aerospace industries, as well as the load-bearing structure of helicopter rotor system. Fatigue fracture, accounting for over 80% of the load-bearing failure, is significantly influenced by the final surface integrity of the parts [2].

With respect to the influence of processing technology and parameters on the surface integrity, as well as the surface integrity on the fatigue life of Ti1023, intensive investigations have been carried out. Jawahir et al. [3] presented recent progress in experimental and theoretical investigations on surface integrity in material removal. Mantle et al. [4] studied the surface integrity of high-speed milling γ-TiAl alloy and found that the surface roughness values were typically less than 1.5 μm. Sun et al. [5] observed the influence of end milling parameters on Ti-6Al-4V surface integrity and recommended the influence of milling speed on the surface roughness and surface residual stress in detail. The experimental results showed that the feed rate had a great influence on the surface roughness. The residual compressive stress varied conversely with the change of milling speed and the feed rate. Umbrello et al. [6] reported their research about the surface integrity of AISI52100, and the results showed that with coolant and low cutting speed, the material hardening rate could significantly increase. Schwach et al. [7] studied the white layer on rolling

contact fatigue using acoustic emission technique and found that the fatigue life of components could be verified for six times because of different surface integrity under certain conditions. Javidi et al. [8] investigated how feed rate and nose radius affected the surface integrity and fatigue life in turning. The study showed that the effect of residual stress on fatigue life was more pronounced than that of surface roughness. Youngsik et al. [9] studied the effects of turning feed rate on the surface roughness and fatigue life of high-strength steel. The study found that fatigue life of the specimen decreased when the turning feed rate increased. Jeelani et al. [10] created the relationship between surface integrity and fatigue of Ti-6Al-2Sn-4Zr-2Mo titanium alloy and found that increasing the cutting speed could improve the machined surface quality and the fatigue life of the parts. The results stated above show that, in addition to the material and the structure of the specimen, the finish process and parameters have an important influence on the surface integrity and fatigue performance [11–13].

For the milling of Ti1023, most investigations are focused on the influence of the milling parameters and process conditions on surface integrity. However, the influence on fatigue performance of the specimens is rarely reported. Yao et al. [14] studied the fatigue life resulting from different surface roughness and micro-stress concentration factor of flat test specimens. The results showed that fatigue life decreased sharply with the increase of surface equivalent stress concentration factor. The drawback is that there is no analysis about the milling parameters affecting the fatigue properties or any investigations about the surface microhardness, surface residual stress, and microstructural deformation underneath the machined surface on fatigue performance.

Based on the previous research achievements, the influence mechanism of milling parameters on the surface topography and surface roughness is deeply analyzed. Through the milling experiments, the influence of the finish milling parameters on the machined surface integrity and fatigue life is analyzed, and the influence mechanism of surface roughness, surface microhardness, and surface residual stress on the fatigue life is comprehensively developed [15, 16]. Results show that milling speed v_s is the predominating parameter affecting the fatigue performance of Ti1023 irrespective of the tool wear; the essential reason of which is the surface enhancement caused by surface microhardening rate and the thickness of microstructural deforming layer underneath the machined surface. Although the feed per tooth f_z obviously influences the surface roughness, it has little effect on the surface stress concentration factor. Therefore, f_z is not decisive to the fatigue performance of the specimen. The research results provide guidelines on the optimization of finish milling parameters of Ti1023, as well as a theoretical basis for the anti-fatigue investigation of Ti1023 parts.

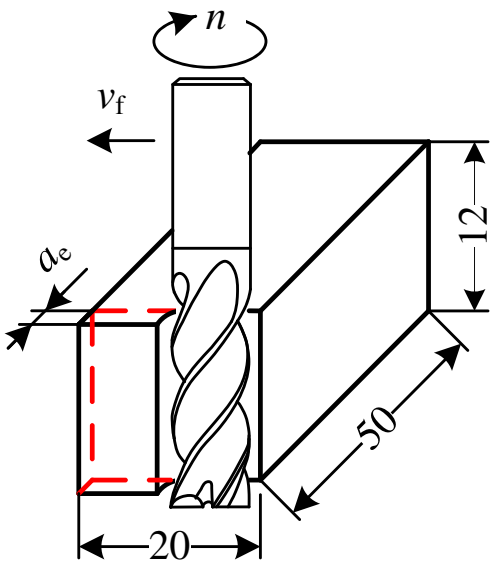

Fig. 1 The schematic diagram of side milling

2 Influence of finish milling parameters on machined surface integrity

2.1 Test material and conditions

All side milling experiments are carried out on a 3-axis CNC milling machine tool, as shown in Fig. 1. Blaser high-speed milling oil is used as the coolant. The sample material is Ti1023 (Ti-10V-2Fe-3Al), solution treated at 750 °C for 2 h, the tensile strength of which is σ_b = 1145 MPa at room temperature. The workpiece dimensions are 50 mm × 20 mm × 12 mm. Eight-millimeter Kennametal solid end milling cutters with four teeth are utilized in all milling experiments.

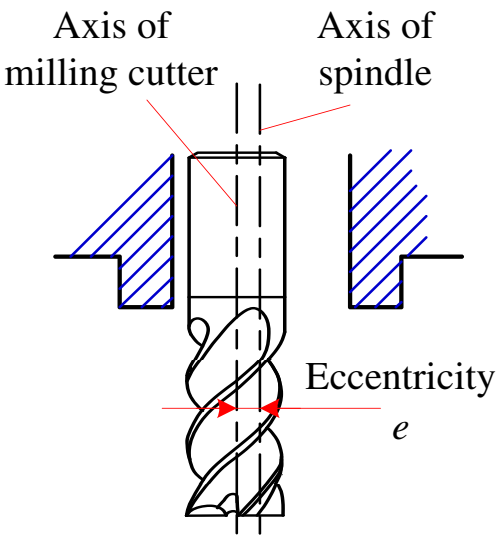

Fig. 2 The schematic diagram of the tool rotation eccentricity

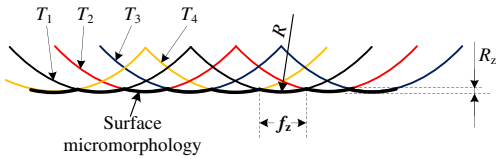

Fig. 3 Motion trajectory simulation of each cutter tooth and surface topography when $e = 0$

The main purpose of finish machining is to ensure the surface quality and machining accuracy and to achieve a certain surface forming rate, which is different from rough machining targeting a high material removal rate. Therefore, the principles of selecting finish machining parameters are also different from that of rough machining. Available research results [11, 14, 17] show that axial cutting depth a_p has little effect on the surface roughness, surface microhardness and surface residual stress. Therefore, the effect of a_p is ignored in the experiments. In addition, the radial cutting depth a_e does not affect the surface forming rate during the finish milling process, which remains almost constant at 0.5 mm. From the above, the axial cutting depth and radial cutting depth are recognized to be unchanged during the milling experiments, with a_p = 12 mm and a_e = 0.5 mm. The milling method and dimensions of surface integrity test specimens are shown in Fig. 1.

2.2 Surface topography formation mechanism of side milling

Side milling method is shown in Fig. 1, and the motion trajectory of spiral cutting edge is a series of extended cycloidal flat surfaces with defined relationships. In the actual machining process, there is a certain amount of rotation eccentricity e after the installation of the tool, as shown in Fig. 2.

If all the parameters are given, the tool rotation eccentricity e has a great influence on the surface topography of milling

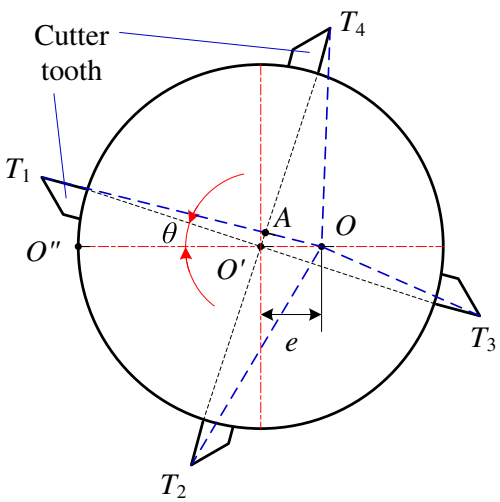

Fig. 4 The relationship between the position of milling cutter and the rotary radius when e ≠ 0

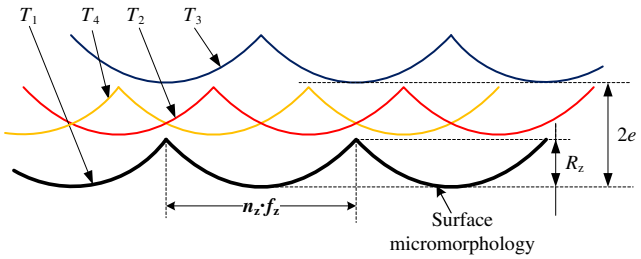

Fig. 5 Typical topography after side milling when $\theta = 0$ and $R_z < 2e$

process. In theory, the effect of each cutter tooth on the milling surface is equal when $e = 0$ and assuming that there is no elastic deformation in the whole process system. When all milling parameters are defined, the surface topography of side milling is almost the same, no matter if it is down milling or up milling, as shown in Fig. 3. According to its geometric relationship, surface maximum residual height $R_z = f_z^2/8R$ [18], where R is the radius of the milling tool.

In the actual machining situation, eccentricity $e \neq 0$ because of the tool clamping error and manufacturing tolerance. In the common range of finish milling parameters, eccentricity e value and the surface maximum residual height R_z value are in the same order of magnitude. Taking milling cutter with four teeth as an example, when the tool is clamped, and assuming that in some cross sections of the tool, the connection between a cutter tooth and the cutter geometry center is $O'T_i$, and the connection between the cutter geometry center and the spindle rotary center is $O'O$. The minimum angle between $O'T_i$ and $O'O$ is the azimuth angle of cutter tooth θ ($0 \leq \theta \leq 45^\circ$). Because the milling cutter edge is helical, the azimuth angle of cutter tooth θ is also different when choosing a different cross-section along the tool axis. The relationships among the machined surface topography, the eccentricity e after installation, the milling parameters f_z, and the milling tool radius R are shown in Fig. 4.

In Fig. 4, where O' is the geometry center point of the milling cutter, O is the spindle rotary center point. θ is the azimuth angle of cutter tooth, and the length of $\overline{O'O}$ is e.

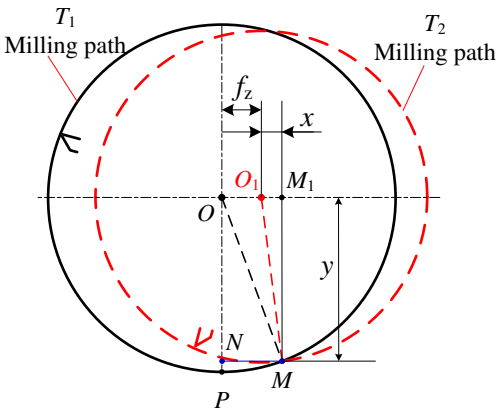

Fig. 6 Location relationship between the motion trajectories of two adjacent cutter teeth

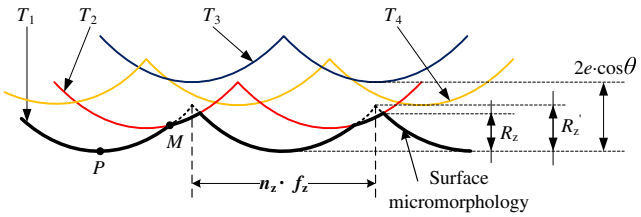

(a) Machined surface with clipping top phenomenon

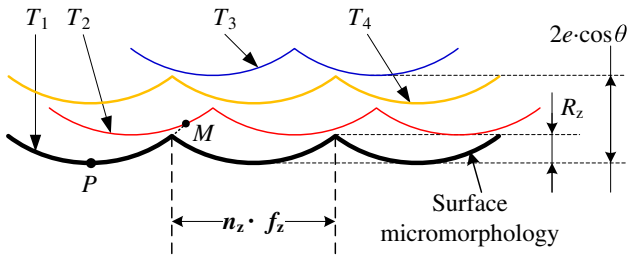

(b) Machined surface with no clipping top phenomenon

Fig. 7 Two typical topography with the increasing of f_z

According to its geometric relationship in Fig. 4, it can be known that $\overline{O'T_1} = \overline{O'T_2} = \overline{O'T_3} = \overline{O'T_4} = R$. Because e is much less than R, $\overline{AT_1} = \overline{O'T_1}$ and $\angle O'OA = \theta$ can be obtained approximately. Then, $\overline{OT_1} = \overline{OA} + \overline{AT_1} = \overline{OA} + \overline{O'T_1}$ and $\overline{OA} = e\cos\theta$ can be obtained. The length of $\overline{OT_1}$, $\overline{OT_2}$, $\overline{OT_3}$, and $\overline{OT_4}$ can be calculated as Eq. (1).

$$\begin{cases} \overline{OT_1} = R + e\cos\theta \\ \overline{OT_2} = R + e\sin\theta \\ \overline{OT_3} = R - e\cos\theta \\ \overline{OT_4} = R - e\sin\theta \end{cases} \tag{1}$$

With the change of e, f_z, and θ, surface topography after the side milling also changes.

The main typical surface topographies are shown below. If $\theta = 0$ and $R_z < 2e$, the surface topography after side milling is shown in Fig. 5.

If θ ranges from 0 to 45°, the motion trajectories of the two milling cutter teeth (T_1 and T_2) with a large rotary radius are shown in Fig. 6. The trajectories of the two teeth inevitably intersect and assuming that one intersection is point M. According to their geometric relationships, Eq. (2) can be obtained.

$$\begin{cases} \left(f_z + \overline{O_1M_1}\right)^2 + \overline{MM_1}^2 = \overline{OM}^2 \\ \overline{O_1M_1}^2 + \overline{MM_1}^2 = \overline{O_1M}^2 \\ \overline{OM} = R + e\cos\theta \\ \overline{O_1M} = R + e\sin\theta \\ \overline{NP} = \overline{OP} - \overline{ON} = \overline{OM} - \overline{MM_1} \end{cases} \tag{2}$$

$\overline{NP}$ could be expressed in the following equation.

$$\overline{NP} = R + e\cos\theta - \sqrt{(R + e\sin\theta)^2 - \left(\frac{(R + e\cos\theta)^2 - f_z^2 - (R + e\sin\theta)^2}{2f_z}\right)^2} \tag{3}$$

Based on the side milling process and the formation mechanism of surface topography, two different typical phenomena could occur. If $\overline{NP} < R_z'$, a typical phenomenon along the cutter feed direction called clipped top will occur, which the surface texture on the peaks will be clipped off. If $\overline{NP} \geq R_z'$, the phenomenon will not occur, as shown in Fig. 7. According to the Eq. (3), it can be concluded that radius of the tool R, clamping eccentricity e, and the feed per tooth f_z work together and lead to this phenomenon.

From the above analysis, the following conclusions can be drawn:

(1) In the practical side milling, there must be an eccentricity e between the cutter geometry center and the spindle rotary center. The increase of eccentricity e leads to that

Table 1 Milling parameters and results of surface roughness

	Milling parameters				Surface roughness R_a (μm)	Surface roughness R_z (μm)	Theoretical value of R_z (μm)
	v_s (m·min^{-1})	f_z (mm·z^{-1})	a_e (mm)	a_p (mm)			
1	20	0.07	0.1	12	0.52	2.26	1.96
2	20	0.10	0.1	12	0.9	3.54	4.00
3	20	0.14	0.1	12	1.38	5.56	4.92
4	30	0.07	0.1	12	0.51	2.24	1.96
5	30	0.10	0.1	12	0.92	3.62	4.00
6	30	0.14	0.1	12	1.23	4.96	4.92
7	40	0.07	0.1	12	0.56	2.37	1.96
8	40	0.10	0.1	12	1.0	3.95	4.00
9	40	0.14	0.1	12	1.32	5.67	4.92

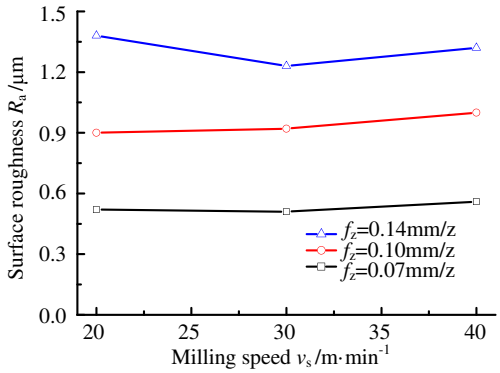

(a) Effect of milling speed on surface roughness R_a

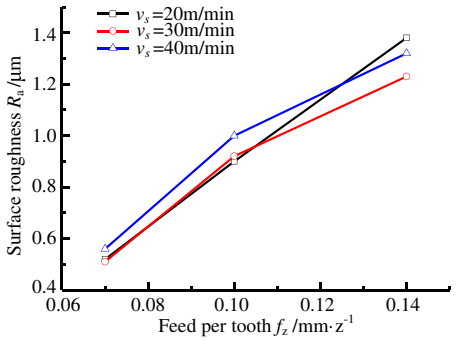

(b) Effect of feed per tooth on surface roughness R_a

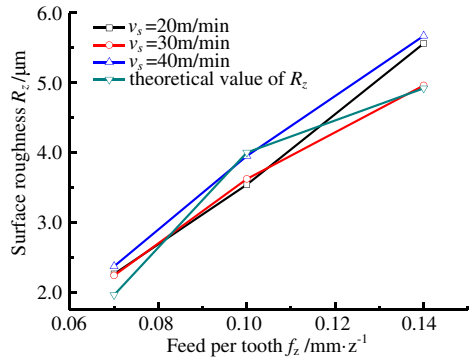

(c) Effect of feed per tooth on surface roughness R_z

Fig. 8 Effect of milling parameters on surface roughness

the cycle of surface texture ranges from f_z in theoretical conditions to $n_z f_z$, as well as the increase of the residual height R_z. Besides, with the change of f_z and θ, R_z changes from $f_z^2/8R$ to $(n_z \cdot f_z)^2/8R$.

(2) In the feed direction, the minimum radius of the surface topography after side milling is approximately equal to the radius of the milling tool, and it does not change with the change of f_z.

2.3 Surface topography and roughness measurement

According to the experimental conditions in Section 2.1 and the analysis results in Section 2.2, the experiments of side

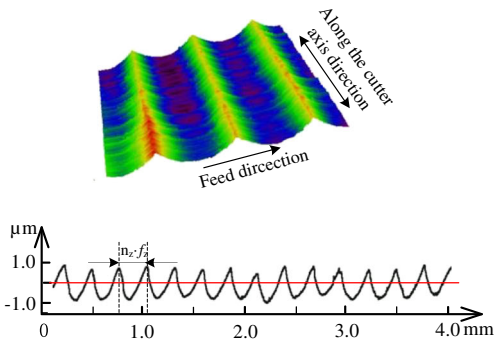

(a) Surface topography when v_s =20 m/min and f_z=0.07 mm/z

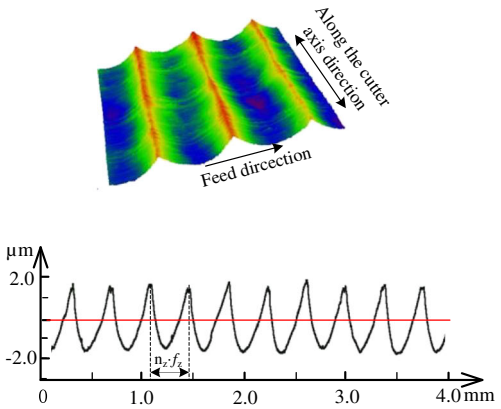

(b) Surface topography when v_s =20 m/min and f_z =0.10 mm/z

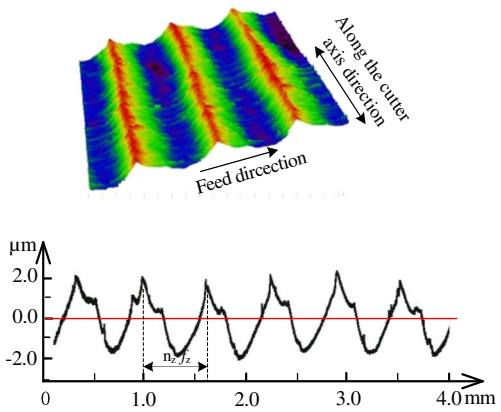

(c) Surface topography when v_s =20 m/min and f_z =0.14 mm/z

Fig. 9 Surface topography and surface texture of side milling

milling of Ti1023 specimens are carried out utilizing the parameters in Table 1. After tool installation, the radical runout of the milling cutter is measured to be about 6 μm. According to the relationship between the eccentricity e and the circular runout of the cutter, e is 3 μm. The surface topography and surface roughness of the specimen are measured by laser scanning microscope (OLYMPUS OLS4100) and Taylor Hobson profiler. Each measuring point is tested five times and averaged for the sake of statistical significance of the measurements.

Table 2 Milling parameters and results of surface microhardness

Number	Milling parameters				Surface microhardnes/HV	Surface microhardening rate (%)
	v_s (m·min^{-1})	f_z (mm·z^{-1})	a_e (mm)	a_p (mm)		
1	20	0.07	0.1	12	418.6	12.5
2	20	0.10	0.1	12	411	10.5
3	20	0.14	0.1	12	400	7.5
4	30	0.07	0.1	12	403	8.3
5	30	0.10	0.1	12	394	5.9
6	30	0.14	0.1	12	385	3.5
7	40	0.07	0.1	12	399.5	7.4
8	40	0.10	0.1	12	387	4.0
9	40	0.14	0.1	12	383	2.9

Theoretical values of surface roughness can be calculated by using the basic theoretical model of roughness $R_z = f_z^2/8R$ [18]. The experimental results are shown in Table 1 and Fig. 8.

From the experimental results above, it could be seen that the theoretical values of the roughness are basically consistent with the experimental measurements of the roughness. In addition, when f_z is a certain value, the influence of v_s on surface roughness is negligible, which is consistent with the theoretical analysis. However, R_a is linear to f_z. When the f_z increases from 0.07 to 0.14 mm/z, R_a increases from 0.5 to 1.4 μm, and R_z increases from 2.2 to 5.7 μm.

Meanwhile, making a comprehensive analysis of surface topography and the curves of surface roughness when v_s is 20 m/min, f_z are 0.07, 0.1, and 0.14 mm/z, the following figures can be obtained.

From the above results, it could be found that the surface texture of the specimen after side milling is obviously periodic. The spacing between two textures could be defined as the distance between two peaks or valleys. From the results, it is obvious that the spacing is $n_z f_z$ instead of f_z. Under the premise of $e = 3$ μm, surface texture on the peaks is clipped off when f_z is 0.14 mm/z, and the clipping top phenomenon is very obvious, which leads to the growth rate of the surface roughness fell slightly. Furthermore, from the profile of the cross section of the surface topography as shown in Fig. 9, it can be seen that the bottom of the profile is a substantially arc shape, and the profile valley radius is substantially equal to the cutter radius, while f_z has no effect on the profile valley radius.

2.4 Surface hardening

Surface hardening is another important indicator of surface integrity because it has a positive influence on fatigue performance, wear resistance, and corrosion resistance of the specimens. The experiments about the influence of different milling parameters on surface hardening are carried out and the microhardness of the machined specimen surface is measured. Each measuring point is tested five times and averaged for the sake of statistical significance of the measurements, as shown in Table 2 and Fig. 10. The hardness of the base material of Ti1023 is about HV372 Mpa.

From the experimental results above, it could be concluded that the milling parameters have a significant influence on Ti1023 surface microhardening rate. In the experiments, the surface hardening phenomenon is prominent and the surface microhardening rate changes between 3 ~ 13%. Compared with f_z, v_s has a great impact on the surface microhardening. When v_s is 20 m/min, f_z increases from 0.07 to 0.14 mm/z, and the surface microhardening rate decreases from 12.5 to 7.5%. While v_s are 30 and 40 m/min, the surface microhardening rate decreases from 8 to 3% with the increase of f_z. Although the reduction degree is basically the same, the absolute value of the machined surface microhardness when v_s is 20 m/min is generally larger than that when v_s are 30 and 40 m/min.

In order to further analyze the influence of v_s on the microstructural deformation of machined surface and the thickness of microstructural deformation, scanning electron microscope (SEM) is used to observe the section of specimens. The results are shown in Fig. 11. It could be concluded that v_s has a great influence on the thickness of microstructural deformation underneath the machined surface layer. When v_s is 20 m/min, the deforming layer is formed underneath the machined surface

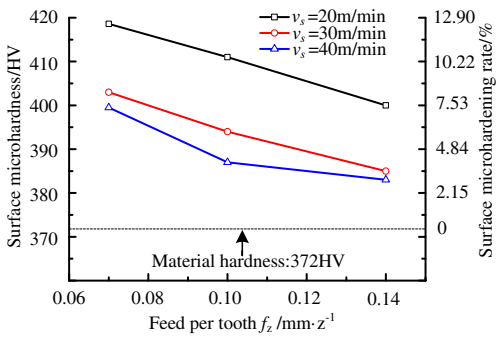

Fig. 10 Effect of milling parameters on surface microhardness

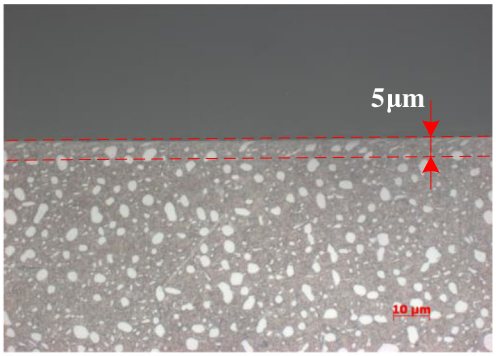

(a) v_s =20m/min, f_z =0.07 mm/z

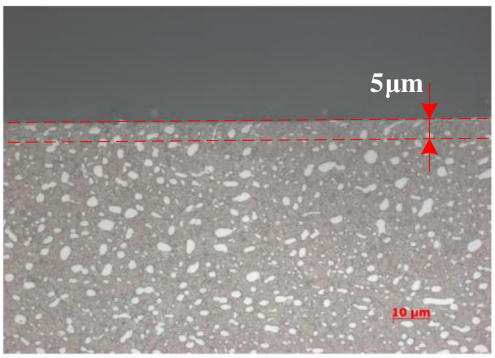

(b) v_s =20m/min, f_z =0.10 mm/z

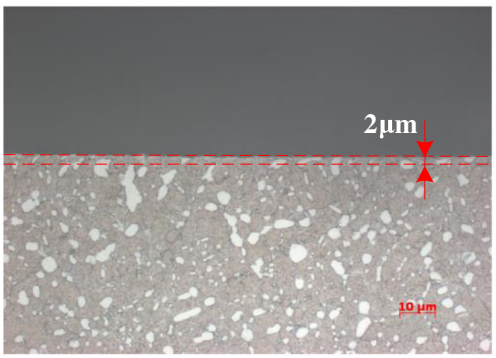

(c) v_s =30m/min, f_z =0.10 mm/z

(d) v_s =40m/min, f_z =0.10 mm/z

Fig. 11 Microstructure of surface layer under different milling parameters

with a thickness of about 5 μm. When v_s is 30 m/min, the thickness of deforming layer is about 2 μm. When v_s is 40 m/min, almost no deformation can be observed closing to the machined surface. The above results also indicate that the influences of cutting parameters on the material deformation of the machined surface.

2.5 Surface residual stress

The influence of surface residual stress on the fatigue life of the specimen has been studied by many researchers [7, 9, 19]. It is generally believed that the residual compressive stress in the machined surface is beneficial to suppress potential risks in terms of crack initiation, propagation, and fatigue failure of end products. However, a quantified or optimal range of the surface residual compressive stress is very difficult to provide and its associated research results are few. Theoretically, when the specimen is subjected to load in milling feed direction, the machined surface residual stress along the feed direction has some effect on the fatigue performance, while the machined surface residual stress perpendicular to the feed direction has no effect on the fatigue performance. Therefore, in the following experiments, only the surface residual stress along the feed direction of the specimen is detected. Utilizing the milling parameters shown in Table 3, the residual stress test on the specimen is carried out. Each measuring point is tested three times and averaged for the sake of statistical significance of the measurements. The experimental results are as shown in Table 3 and Fig. 12.

From the test results shown in Table 3 and Fig. 12, it can be seen that the surface residual stress of Ti1023 after finish milling is compressive stress. Within the range of experimental parameters, the compressive stress ranges from −87 to −180 MPa. From the general trend, the value of the residual stress goes up with the increase of v_s and f_z. When v_s is 20 m/min, with the value of f_z increasing from 0.07 to 0.14 mm/z, the machined surface residual stress increases from −93.49 to −110.47 MPa, whose increase range is approximately 18%. When v_s is 30 and 40 m/min, with the increase of f_z, the residual stress of the machined surface increases approximately 73.7 and 84%, respectively. The increase is significantly greater than that when v_s is 20 m/min.

3 Effect of finish milling parameters on fatigue performance of specimens

3.1 Fatigue performance test specimen

There are mainly two kinds of typical fatigue specimen with rectangular and circular cross section. Theoretically, rectangular cross-sectional specimen is more suitable for studying the influence of finish surface integrity on fatigue performance. In the case of certain cross-sectional area, the influence of rectangular surface quality on the fatigue life can be expanded by adjusting the length of the two rectangle sides, and it is easier

Table 3 Milling parameters and results of surface residual stress

Number	Milling parameters				Surface residual stress σ_H (MPa)
	v_s (m·min^{-1})	f_z (mm·z^{-1})	a_e (mm)	a_p (mm)	
1	20	0.07	0.1	12	−93.49
2	20	0.10	0.1	12	−100.24
3	20	0.14	0.1	12	−110.47
4	30	0.07	0.1	12	−87.57
5	30	0.10	0.1	12	−109.88
6	30	0.14	0.1	12	−151.93
7	40	0.07	0.1	12	−98.08
8	40	0.10	0.1	12	−149.16
9	40	0.14	0.1	12	−180.57

to observe the influence of different machining parameters and surface integrity on fatigue performance. However, there must exist sharp corners in rectangular specimens, which have influence on the fatigue performance directly. In order to reduce the impact of sharp corners, generally machining chamfers of 45 degree angle or round corners is used, and it should be polished or shot peened to assure the crack initiation have their origin in the area of the milling surface. At the same time, it is very difficult to make sure of the chamfers' stability with the thickness decreasing of the specimen, which results in the great dispersion of specimen fatigue performance. Considering all the conditions above, the fatigue life specimens of similar circular section are utilized, as shown in Fig. 13. The cross section is 60-sided polygon and of which side length is about 0.26 mm (when utilizing side milling, the influence of the axial cut depth on the surface integrity can be ignored). The angle between the two adjacent sides is 6 ° and the stress concentration of the corner is negligible, so the impact of sharp corners on the fatigue life of the specimen can be ignored.

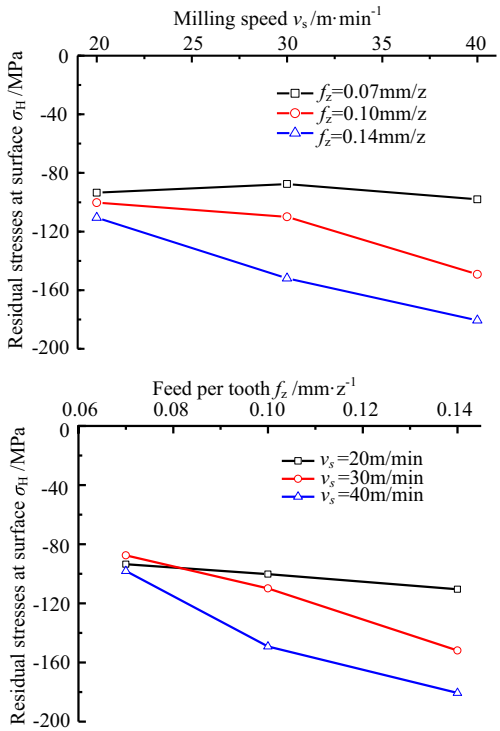

Fig. 12 Effect of milling parameters on surface residual stress

3.2 Fatigue performance test experiments

Considering the influence of milling parameters on surface integrity and experimental results, the method of side milling is shown in Fig. 13. All fatigue experiments are carried out on a GPS100 high frequency tensile fatigue testing machine, as shown in Fig. 14. The working frequency is 80–250 Hz; the loading waveform is sine wave. The maximum average load is 100 KN and the maximum alternating load is 50 KN. Based on the strength limit of the material, the maximum tensile load of fatigue specimens is set to be 980 Mpa, and the cyclic stress ratio r is 0.1. The clamping of fatigue specimens and their failure modes are shown in Fig. 15. The milling parameters are utilized to machine the fatigue specimens and the experimental results are shown in Table 4 and Fig. 16.

As can be seen in Fig. 16, in the case that f_z has a certain value, with the increase of v_s, the fatigue life of the specimen is greatly reduced. When v_s is 20 m/min, the fatigue life is two times than that when v_s is 30 and 40 m/min. However, the

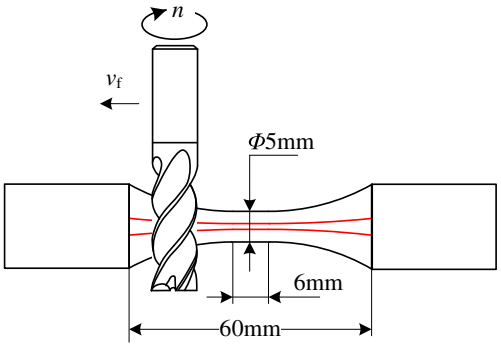

Fig. 13 Fatigue specimens of side milling

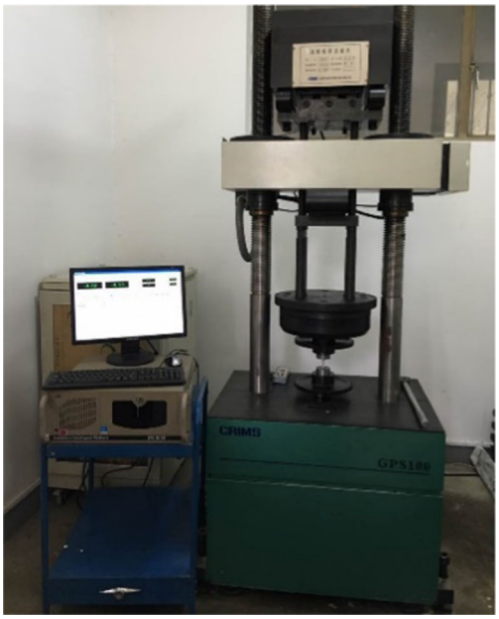

Fig. 14 The high frequency tensile fatigue testing machine

fatigue life of the specimens is not obviously different between 30 and 40 m/min. Furthermore, in the case of a certain v_s, f_z has little effect on the fatigue life of the specimens, and the fatigue life of the specimens is basically unchanged when f_z increases from 0.07 to 0.14 mm/z.

3.3 Discussion

From the experimental results above, it can be known that milling parameters have a great influence on the fatigue life of specimens. However, the influence of v_s and f_z on the fatigue life of specimens is different. The essential reason should be analyzed from the surface integrity after side milling.

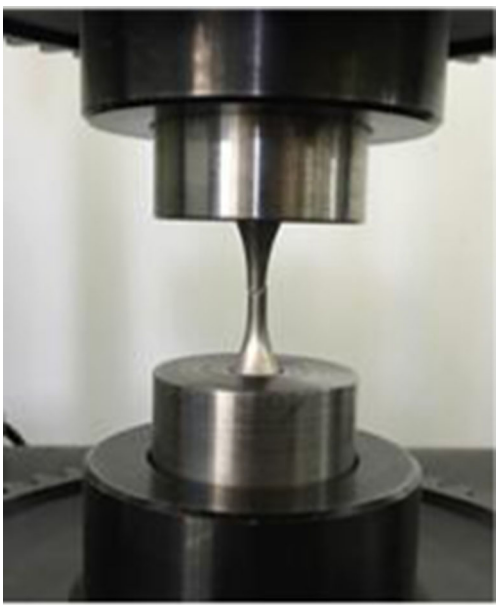

Fig. 15 The clamping and failure mode of fatigue specimens

(1) The surface roughness is one of the important factors that affect the fatigue life of the specimens. Many studies show that, in general, the bigger the surface roughness values are, the more serious the stress concentration and the poorer the anti-fatigue performance are. That is because that the surface roughness can cause stress concentration, and the crack initiation often have their origins in the area where stress concentration happens [19]. When the workpiece is subjected to tensile loading and the machined surface topography is characterized by a continuous gap, the empirical equation for estimation of the fatigue stress concentration factor can be expressed by R_z as follows [20]:

$$Kt = 1 + 2\sqrt{\lambda \mathrm{Rz} / \rho}$$

where ρ is the curvature radius at the bottom of the gap; λ refers to the ratio between spacing and depth of the gap. For the machined surface, λ is defined as $\lambda = 1$ generally [21]. In this paper, the surface topography of side milling is a continuous adjacent arc gap, as shown in Fig. 7, which is suitable for the empirical formula. At this time, the curvature radius ρ is about equal to the tool radius R. By calculating, within the range of these experimental parameters, the surface maximum residual height R_z substantially changes from 2.2 to 5.7 μm, while the radius of the milling cutter is 5 mm. Therefore, the micro stress concentration factor K_t along the feed direction does not change with the changing of f_z. Therefore, in the range of experimental parameters, the micro local stress concentration caused by the surface roughness is basically the same, since R_z/ρ is very small. Thus, f_z has little effect on the fatigue life of specimens;

(2) The surface microhardening rate results show that, in the case of a certain f_z, the surface microhardening rate of specimens after processing by the milling speed of 20 m/min is about 1.5–2.6 times than that processed by the milling speed of 30 and 40 m/min, and all the microhardening rates are more than 7.5%. At the same time, when v_s is 20 m/min, the thickness of microstructural deforming layer underneath the machined surface is about 5 μm. However, when v_s are 30 and 40 m/min, the thicknesses of deforming layer are about 2 and 0 μm, respectively. Furthermore, the results of surface residual stress experiments show that, in the case of a certain v_s, the maximum increase of the residual stress at the

Table 4 Milling parameters and results of fatigue tests

Number	Milling parameters				Number of cycles to failure N
	v_s (m·min^{-1})	f_z (mm·z^{-1})	a_e (mm)	a_p (mm)	
1	20	0.07	0.1	0.2	108,880
2	20	0.10	0.1	0.2	123,040
3	20	0.14	0.1	0.2	95,640
4	30	0.07	0.1	0.2	54,800
5	30	0.10	0.1	0.2	45,135
6	30	0.14	0.1	0.2	53,950
7	40	0.07	0.1	0.2	44,800
8	40	0.10	0.1	0.2	40,282
9	40	0.14	0.1	0.2	40,156

machined surface is only about 80 Mpa with the change of f_z. Although a proper surface residual compressive stress can increase the fatigue life, the improvement is relatively weak because the absolute values of surface residual compressive stress are small. Therefore, it is believed that the surface microhardening rate and the thickness of microstructural deforming layer underneath the machined surface are the main factors that influence the fatigue life of the specimen, while the influence of surface roughness along the feed direction and surface residual stress on the fatigue life of the specimen, is not obvious during side milling of Ti1023.

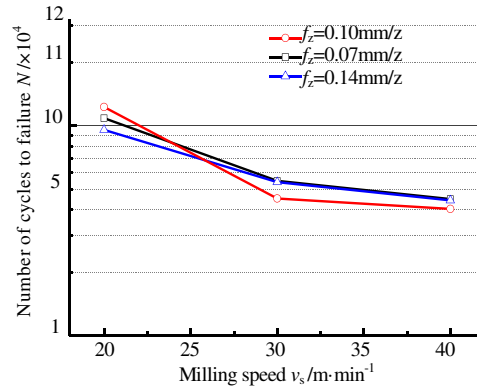

(a) Number of cycles to failure changing with v_s

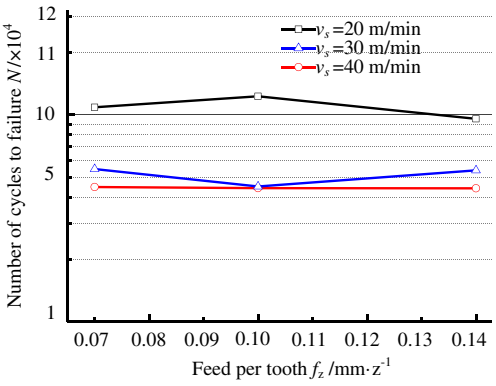

(b) Number of cycles to failure changing with f_z

Fig. 16 Effect of milling parameters on fatigue life of specimens

4 Conclusions

(1) When the tool rotating axis is not coincident with the spindle rotating axis, namely the tool runout is not 0, the surface texture of the specimen is obviously periodic after side milling. The spacing of surface texture is $n_z f_z$ rather than theoretical f_z. From the results above, it can be concluded that surface texture of the specimen after side milling is clear periodicity, and the distance between the lines is $n_z f_z$, rather than theoretical f_z. Meanwhile, R_a is linear to f_z.

(2) Compared with f_z, v_s has a greater impact on the machined surface hardening. In the case that v_s is 20 m/min, when f_z increases from 0.07 to 0.14 mm/z, the surface microhardening rate decreases from 12.5 to 7.5%. While v_s are 30 and 40 m/min, the surface microhardening rate decreases from 8 to 3% with the increase of f_z. At the same time, when v_s is 20 m/min, the thickness of microstructural deforming layer underneath the machined surface is about 5 μm. However, when v_s are 30 and 40 m/min, the thicknesses of deforming layer are about 2 and 0 μm, respectively.

(3) Within the experimental parameters, the surface residual stress of Ti1023 after finish milling is compressive stress. The numerical value of the residual stress increases with the increase of v_s and f_z, and the compressive stress changes in the range of −87 to −180 MPa. At the same time, when v_s is 20 m/min, the numerical value of the residual stress at the machined surface increases about 18%, which is smaller than that when v_s are 30 and 40 m/min.

(4) It is presented that the surface microhardening rate and the thickness of microstructural deforming layer underneath the machined surface of Ti1023 side milling are the

main factors that influence the fatigue life of the specimen. Meanwhile, the influences of surface roughness along the feed direction and surface residual stress on the fatigue life are not obvious when utilizing side milling. Therefore, based on the experimental results of fatigue life, v_s should be chosen preferentially, and the microhardening rate of the surface and the deformation depth of the surface texture should be improved as far as possible when optimizing the parameter of Ti1023 side milling. At the same time, under the circumstance that the design requirements of workpieces are satisfied, f_z should be increased as much as possible in order to improve the finish milling efficiency.

References

1. Wang MJ, Meng XJ, Liao ZQ, Shi-Kai LI (2009) Present state of research on Ti1023 titanium alloy (in Chinese). Dev Appl Mater 24(5):66–69
2. Tao CH, Zhong PD, Wang RZ (2008) Failure analysis and prevention for rotor in aero-engine (in Chinese). National Defense Industry Press, China
3. Jawahir IS, Brinksmeier E, M'Saoubi R, Aspinwall DK, Outeiro JC, Meyer D (2011) Surface integrity in material removal processes: recent advances. CIRP Ann - Manuf Technol 60(2):603–626
4. Mantle AL, Aspinwall DK (2001) Surface integrity of a high speed milled gamma titanium aluminide. J Mater Process Technol 118(1–3):143–150
5. Sun J, Guo YB (2009) A comprehensive experimental study on surface integrity by end milling Ti–6Al–4V. J Mater Process Technol 209(8):4036–4042
6. Umbrello D, Pu Z, Caruso S, Outeiro JC, Jayal AD, Dillon OW (2011) The effects of cryogenic cooling on surface integrity in hard machining. Procedia Eng. 19(3):371–376
7. Schwach DW, Guo YB (2006) A fundamental study on the impact of surface integrity by hard turning on rolling contact fatigue. Int J Fatigue 28(12):1838–1844
8. Javidi A, Rieger U, Eichlseder W (2008) The effect of machining on the surface integrity and fatigue life. Int J Fatigue 30(30):2050–2055
9. Choi Y (2015) Influence of feed rate on surface integrity and fatigue performance of machined surfaces. Int J Fatigue 78:46–52
10. Jeelani S, Ramakrishnan K (1983) Subsurface plastic deformation in machining 6Al-2Sn-4Zr-2Mo titanium alloy. Wear 85(1):121–130
11. Yao CF, Wu DX, Tan L, Shi K, Yang Z (2013) Effects of cutting parameters on surface residual stress and its mechanism in high-speed milling TB6. Proc Inst Mech Eng Part B: J Eng Manuf 227(4):483–493
12. Zhou ZT, Chen ZT, Xiong XY, Xu Y (2014) Experiment on surface integrity of side milling titanium TB6 (in Chinese). J B Univ Aeronaut Astronaut 40(6):849–854
13. Durul U, Tugrul O (2011) Machining induced surface integrity in titanium and nickel alloys: a review. Int. J Mach Tools Manuf 51(3): 250–280
14. Yao CF, Wu DX, Jin QC, Huang XC, Ren JX, Zhang DH (2013) Influence of high-speed milling parameter on 3D surface topography and fatigue behavior of TB6 titanium alloy. Trans. Nonferrous Met. Soc. China 23(3):650–660
15. Safari H, Sharif S, Izman S, Jafari H (2015) Surface integrity characterization in high-speed dry end milling of Ti-6Al-4V titanium alloy. Int J Adv Manuf Technol 78(1):651–657
16. Souto-Lebel A, Guillemot N, Lartigue C, Billardon R (2011) Characterization and influence of defect size distribution induced by ball-end finishing milling on fatigue life. Procedia Eng 19(1):343–348
17. Li W, Guo YB, Barkey ME (2011) Tool Wear Influence on Surface Integrity and Fatigue Life of Hard Milled Surfaces, ASME/STLE 2011 International Joint Tribology Conference. p. 75–77
18. Wyen CF, Jaeger D, Wegener K (2013) Influence of cutting edge radius on surface integrity and burr formation in milling titanium. Int J Adv Manuf Technol 67(1):589–599
19. Gao YK, Li XB, Yang QX, Yao M (2007) Influence of surface integrity on fatigue strength of 40CrNi2Si2MoVA steel. Mater Lett 61(2):466–469
20. Suraratchai M, Limido J, Chieragatti R (2008) Modelling the influence machined surface roughness on the fatigue life of aluminium alloy. Int J Fatigue 30(12):2119–2126
21. Arola D, Williams CL (2002) Estimating the fatigue stress concentration factor of machined surface. Int J Fatigue 24(9):923–930